AIP | Physics of Fluids

Dynamic spreading on pillar-arrayed surfaces: Viscous resistance versus molecular friction

Quanzi Yuan, Xianfu Huang, and Ya-Pu Zhao

Citation: Physics of Fluids (1994-present) **26**, 092104 (2014); doi: 10.1063/1.4895497
View online: http://dx.doi.org/10.1063/1.4895497
View Table of Contents: http://scitation.aip.org/content/aip/journal/pof2/26/9?ver=pdfcov
Published by the AIP Publishing

PHYSICS OF FLUIDS **26**, 092104 (2014)

Dynamic spreading on pillar-arrayed surfaces: Viscous resistance versus molecular friction

Quanzi Yuan, Xianfu Huang, and Ya-Pu Zhao[a)]
State Key Laboratory of Nonlinear Mechanics, Institute of Mechanics, Chinese Academy of Sciences, Beijing 100190, People's Republic of China

(Received 20 June 2014; accepted 29 August 2014; published online 12 September 2014)

The dynamic spreading of a liquid droplet on micropillar-arrayed surfaces is experimentally investigated. A theoretical model is proposed to include energy dissipations raised from both the viscous resistance at mesoscale and the molecular friction at microscale in the triple-phase region. The scaling laws and spreading shape of the droplet change with the variation of the liquid viscosity because of the competition between these two mechanisms of energy dissipations at the moving contact line. The Laplace pressures at the interior corner and at the wavy contact line are the answers to the excess driving energy and the superwetting on pillar-arrayed surfaces. The formation and evolution of the bulk and the fringe are also analyzed in detail. Our results may help to understand the wetting dynamics on microtextured surfaces and assist the future design of engineered surfaces in practical applications. © *2014 AIP Publishing LLC*. [http://dx.doi.org/10.1063/1.4895497]

I. INTRODUCTION

The spreading of a droplet on a smooth substrate has been intensively studied for decades.[1–3] Considering a droplet of radius R_0 be much smaller than the capillary length $L_{CA} = \sqrt{\gamma_{LV}/\rho g}$ (γ_{LV}, ρ, and g are, respectively, the liquid-vapor interface energy, liquid density, and the gravitational acceleration), the surface tension drives the droplet to spread (Fig. 1). There are essentially two theoretical models to interpret the energy dissipation at the moving contact line (MCL) and therefore leading to two scaling laws. In the framework of the hydrodynamics, the energy dissipation caused by viscous resistance takes place at mesoscale L. L is the size of mesoscale region, which is estimated as $L \sim \mathrm{Ca} \cdot R/\theta$, base on where the profile turns from concave to convex, where $\mathrm{Ca} = \mu U/\gamma_{LV}$, R, μ, U, and θ are, respectively, the capillary number, instant radius, viscosity, spreading velocity, and instant contact angle (Fig. 1(b)).[4] A rapid bending of the meniscus connects the quasi-static macro- and micro-scale L_m, resulting a viscous dissipation of $D_{vis} \sim \mu \ln(R_0/L_m)\, U^2/\theta$. L_m is a microscopic neighborhood of the contact line (of the size of nanometer), where molecular details matter and a molecular description needs to be adopted. The consequent scaling law of the spreading radius is $R \sim t^{1/10}$, where t is the spreading time.[5] In the framework of molecular kinetic theory (MKT), the energy dissipation caused by adsorption and desorption of liquid molecules on a solid occurs at molecular scale L_m (Fig. 1(c)).[6] The liquid molecules jump between the adsorption sites separated by a distance λ with a frequency κ_0 in the triple-phase region, resulting a molecular dissipation of $D_{mol} \sim \zeta U^2$, where $\zeta = k_B T/\kappa_0 \lambda^3$, k_B, and T are, respectively, the coefficient of molecular friction, the Boltzmann constant, and absolute temperature. The consequent scaling law is $R \sim t^{1/7}$. These two models include energy dissipations at different scales, respectively. However, more evidences show that both viscous resistance at mesoscale and the molecular friction at microscale play a part in energy dissipation at MCL.[7] Thus, Brochard-Wyart and de Gennes[8] and Ruijter *et al.*[9] proposed a combined model to take account of both factors. The derived scaling law is $R \sim t^n$ and corroborated by experiments and simulations, where $1/10 \le n \le 1/7$ is the scaling exponent.

[a)] Author to whom correspondence should be addressed. Electronic mail: yzhao@imech.ac.cn

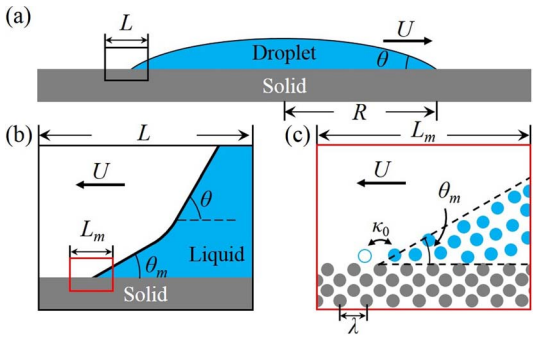

FIG. 1. (a) A spreading droplet partially wets a smooth solid surface, where θ, R, and U are the instant contact angle, radius, and velocity of the droplet, respectively. (b) Hydrodynamics: viscous resistance at mesoscale L. (c) Molecular kinetic theory: molecular friction at microscale L_m. θ_m, λ, and κ_0 are the microscopic contact angle, the distance between adsorption sites on the solid surface, and the equilibrium frequency of liquid molecules, respectively.

When the smooth substrate is patterned with micropillars, its intrinsic wettability is changed by the surface roughness (the ratio between the actual and projected surface areas),[10] resulting in new phenomena such as superwetting,[11,12] drag reduction,[13,14] wetting transition,[15,16] etc. Because of potential applications in fog-harvesting,[17] biomedicine,[18] anti-icing,[19] microfluidics,[20] etc., a surge of interest in the dynamic spreading on micropillar-arrayed surfaces has emerged. However, the wetting dynamics on pillar-arrayed surfaces is far from well understood and the scaling law is still debated. The pioneering work of Hasimoto estimated the viscous resistance of the pillars to the fluid by idealizing the pillars as infinitely long cylinders.[21] Based on the Washburn law, Ishino *et al.*[22] considered viscous dissipation on the substrate and the side walls, and obtained two extreme regimes for short and tall pillars, respectively. Then, Srivastava *et al.*[23] and Xiao and Wang[24] developed Ishino's model and got a more accurate exponent. Taking account of the viscous dissipation in the triple-phase region, dynamic wetting in the early stage of a liquid film with/without bulk droplet and the entire drop footprint on pillar-arrayed surfaces were studied.[25] Yuan and Zhao proposed a scaling law taking account of the molecular friction at the MCL.[12] Recently, Semprebon *et al.* did elegant experiments and simulations to study the pinning and wicking of a liquid meniscus in a square array of pillars, and proposed a criteria for spontaneous film formation.[26] When liquid spreads on a smooth solid, a mesoscale intermediate region of size L is used to connect the macroscale and microscale region as shown in Fig. 1. When liquid spreads on a micropillar-arrayed surface, a new lengthscale of the micropillars is introduced to the system, which is just about L and would lead to new competitions between viscous resistance and surface forces at mesoscale, as well as induce new phenomena and mechanisms. On the one hand, the pillars provide excess energy to drive the liquid to spread faster. On the other hand, the excess solid-liquid interface results in excess contact line length, which dissipates more energy at both meso- and micro-scale in the triple-phase region. There lacks a systematic and multiscale study on the dynamic spreading of a droplet on micropillar-arrayed surfaces.

In this paper, we first carry out experiments of the spreading of droplets with varied viscosity on micropillar-arrayed surfaces. The liquid structures during the superwetting are revealed and analyzed in detail. Then, theoretical models including energy dissipations at both meso- and micro-scale are constructed to interpret underlying physical mechanisms. Competition between the lengthscales of the droplet and the pillars, as well as competition between the viscous resistance and the molecular friction result in changes in the scaling law and the spreading shape.

II. EXPERIMENTAL METHODS

The preparation of micropillar-arrayed surfaces was carried out in two steps. First, the negative pattern was fabricated on a silicon wafer using conventional photolithography followed by a deep reactive ion etching process at the Institute of Microelectronics, Peking University (Fig. 2(d)). Then,

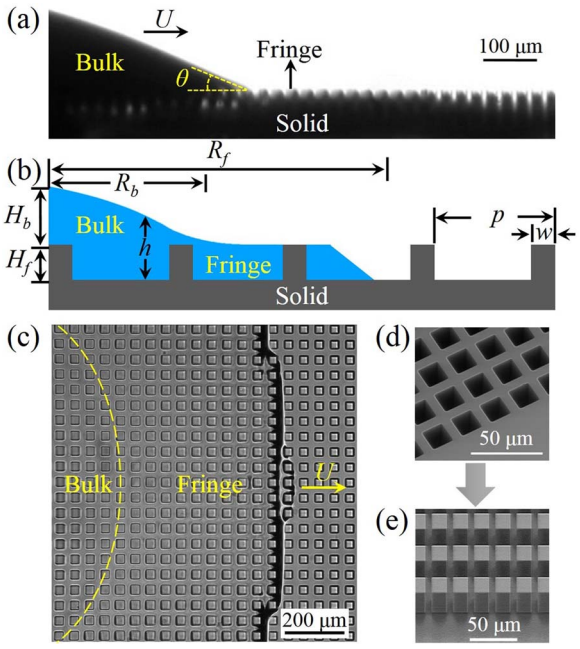

FIG. 2. (a) Side view, (b) top view of experiments, and (c) illustration of a droplet on a pillar-arrayed surface. Scanning electron microscope (SEM) images of (d) the silicon mould and (e) the PDMS pillars. R_b, H_b, and R_f are the radius and height of the bulk droplet, and the average fringe radius, respectively. w, H_f, and p are the pillar size, the pillar height, and the period of the pillars, respectively.

TABLE I. Parameters of the pillar-arrayed surfaces ($H_f = 30$ μm).

Sample	1	2	3	4	5	6
w (μm)	5	5	10	5	15	15
p (μm)	25	20	30	15	35	20
$\phi_s = w^2/p^2$	0.04	0.06	0.11	0.11	0.18	0.56
$ro = 1 + 4wH_f/p^2$	1.96	2.50	2.33	3.67	2.47	5.50

TABLE II. Properties of different silicone oils (KF-96, Shin-Etsu).[27]

Viscosity μ (mPa s)	Surface tension γ_{LV} (mN/m)	Density ρ (kg/m^3)
5	19.7	910
50	20.7	959
500	21.1	970

the silicon pattern was used as a mould for patterning the Polydimethylsiloxane (PDMS) shown in Fig. 2(e). Topological parameters [w, p, H_f], surface roughness ro and density of roughness ϕ_s of these experimental samples were varied and listed in Table I. The surface roughness is defined as the ratio between the actual and projected surface areas and $ro = 1 + 4wH_f/p^2$ for square pillars. The larger the ro is, the larger the actual surface area is. The density of roughness is defined as the ratio of the area of the top faces to the total base area and $\phi_s = w^2/p^2$ for square pillars. Because the pillar heights of all the samples are the same, the smaller ϕ_s is, the larger the space among the pillars is. The liquid was chosen to be silicone oil with different viscosities μ, but similar surface tensions γ_{LV} and densities ρ (Table II). The contact angle of the silicone oil on PDMS is zero. Since the capillary length for silicone oil is $L_{CA} = \sqrt{\gamma_{LV}/(\rho g)} \approx 1.48$ mm, the ratio R_0/L_{CA} is less than 17% (initial

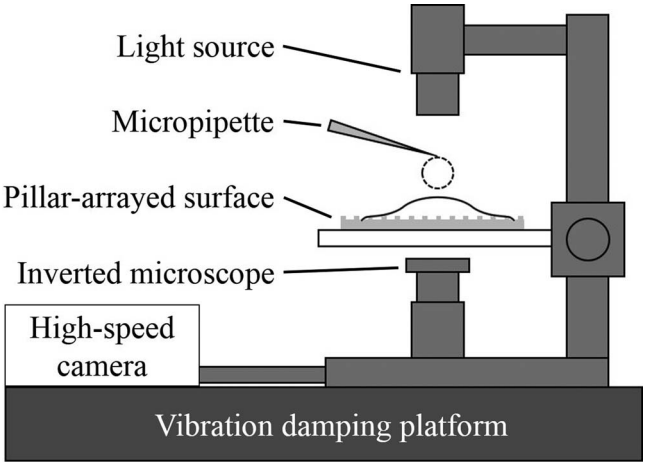

FIG. 3. A schematic of the experimental setup.

droplet radius $R_0 \sim 0.25$ mm), which makes the surface tension take priority over gravity in the wetting process. The liquid motion was captured using an inverted high-magnification microscope (IX71, Olympus) and a high-speed camera (Hotshot 512 sc, NAC) at a frame rate up to 60 000 fps. The schematic of experimental setup is shown in Fig. 3.

III. RESULTS AND DISCUSSION

A. Experimental results

When a droplet was brought into contact with a micropillar-arrayed surface, the droplet spread into two parts (Fig. 2). The lower part, namely the fringe, penetrated into the gaps among the pillars. The upper part, namely the bulk, spread on the base of the fringe and supplied the expansion of the fringe. We captured snapshots during this process between two columns of pillars and generated corresponding three-dimensional spreading profiles of the liquid based on the Fresnel equations shown in Fig. 4. (Details of three-dimensional spreading profiles are described in the Appendix.[39]) When the droplet was brought into contact with the substrate, the liquid wedge began to spread (Fig. 4(a)). The height of the pillars is 30 μm, hence the liquid below 30 μm is the fringe and that above 30 μm is the bulk. The fringe penetrated into the gaps among the pillars with a velocity faster than the bulk (Fig. 4(b)). With the increase of the distance between the fringe and the bulk, a transition region gradually formed to link the liquid among the pillars and the liquid wedge (Fig. 4(c)). When the fringe flowed over the pillars, the liquid also spread fast along the height of the pillars and resulted in a ridge of liquid above the pillar top and a meniscus in the transition region (Fig. 4(d)). In this way, the fringe separated from the droplet and penetrated among the pillars.

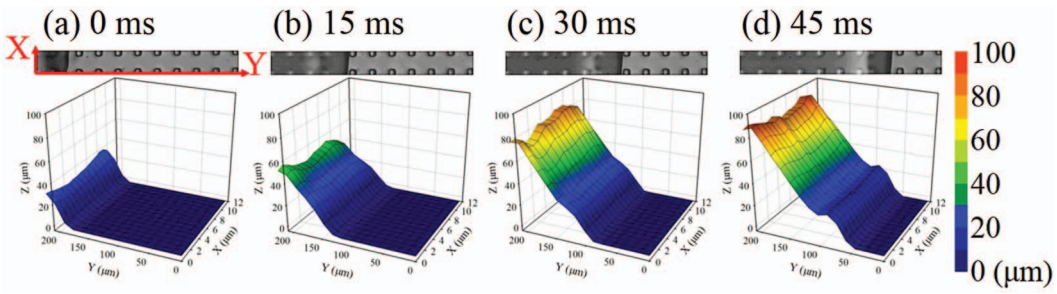

FIG. 4. Sequence snapshots and three-dimensional spreading profiles of liquid ($\mu = 5$ mPa s) on pillar-arrayed surfaces (sample 2 in Table I). The color represents the height of the liquid.

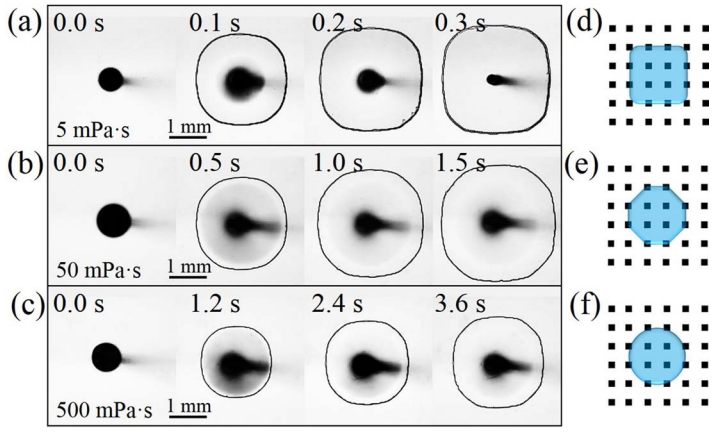

FIG. 5. Experimental snapshots of the spreading of a droplet with viscosities of (a) 5 mPa s, (b) 50 mPa s, and (c) 500 mPa s on the lyophilic pillars (sample 1 in Table I). In the projection of the liquid, the dark area means the interface is inclined with the substrate at a large angle, while the bright area means the interface is parallel to the substrate. (d)-(f) Illustration of the square, octagonal, and circle shape of the fringe.

The dynamic behaviors of the fringe in our experiments are consistent with the previous numerical simulations.[26]

The dynamic processes of droplets with different viscosities spreading on micropillar-arrayed surfaces are shown in Fig. 5. At a first glance of Fig. 5, the liquid flowed in a viscosity-dependent capillary velocity, so a droplet with a lower viscosity spread faster. The bulk expanded on the base of the fringe, whose top was chemically and topologically smooth.[28,29] Thus, the flow velocity of the bulk was isotropic, and its projection was always a circle as shown in Figs. 2(b) and 5. Observed under the microscope, the dark area means there is an interface inclined with the substrate, while the bright area means the interface is parallel to the substrate. In fringe region, the liquid surface is nearly parallel to PDMS. Most of incident energy transmits through liquid and PDMS, and only small part of energy is reflected. In the contact line region, the liquid surface is inclined at a large angle with the substrate. Therefore, little incident energy transmits resulting in a dark outline at the contact line region. The fringe shape was influenced by its viscosity. The fringe propagated ahead of the bulk in the forest of micropillars. The pillars accelerated the approaching MCL, and pinned the leaving MCL. The distance between pillars varied with flow direction, making the corresponding energy dissipation to be anisotropic.[30] Therefore, the fringe spread in a direction-dependent velocity.[31] Furthermore, the velocity was symmetric about the orthogonal and diagonal directions because of the arrangement of the pillars (Fig. 2(d)). In this way, the fringe evolved into an octagonal shape (Figs. 5(b) and 5(e)). For a liquid with a lower viscosity, its velocity and corresponding inertial force were larger. The fringe easily overcame the energy barrier along the diagonal direction of the pillars, becoming approximately a square (Figs. 5(a) and 5(d)). For a liquid with a higher viscosity, its velocity and corresponding inertial force was smaller. The MCL tried to achieve a kinetic balance in all directions, making the fringe roughly a circle (Figs. 5(c) and 5(f)).

To reveal the spreading rules on the pillar-arrayed surface, we quantitatively recorded the evolution of the fringe area S with respect to time shown in Fig. 6. The scaling law of the fringe area varied with liquid viscosity. In Fig. 6(a), the fringes with $\mu = 5$ mPa s evolved in a scaling law of about $S \sim t^{2/3}$. When the liquid viscosity is small, the molecular friction at microscale is the main source of energy dissipation. In Fig. 6(c), the fringes with $\mu = 500$ mPa s evolved in a scaling law of about $S \sim t^{1/2}$. When the liquid viscosity is large, the viscosity resistance at mesoscale is the main source of energy dissipation. The scaling index of the liquid with $\mu = 50$ mPa s was between 1/2 and 2/3 (Fig. 6(b)). In this situation, the viscous resistance together with the molecular friction contributes to the energy dissipation, so the scaling law depends on their proportion in the total energy dissipation. The physical mechanisms behind the scaling laws will be analyzed and discussed in Sec. III B. The corresponding spreading velocity $U \sim t^{-2/3}$ for $\mu = 5$ mPa s and

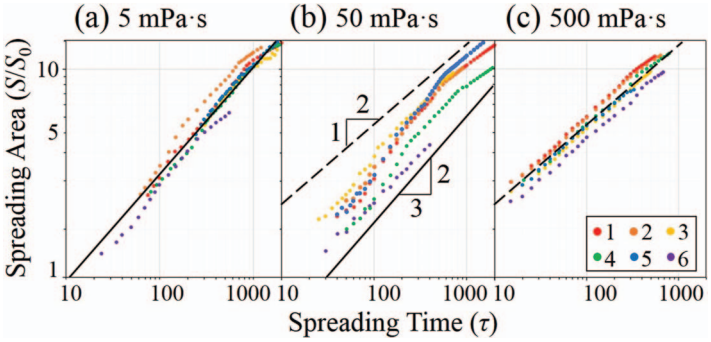

FIG. 6. The evolution of the fringe area with respect to time of droplets with viscosities of (a) 5 mPa s, (b) 50 mPa s, and (c) 500 mPa s on pillar-arrayed surfaces, respectively. S and S_0 represent the instant and initial area of the fringe, respectively. $\tau = t\gamma_{LV}/\mu R_0$ is the dimensionless spreading time. The colored points represent data for sample 1–6 in Table I. The dashed and solid lines represent the scaling laws $S/S_0 \sim \tau^{1/2}$ and $S/S_0 \sim \tau^{2/3}$, respectively.

$U \sim t^{-3/4}$ for $\mu = 500$ mPa s. So, we plotted the evolution of spreading velocity with respect to time shown in Fig. 7 and found that the experiments obey the calculated scaling laws, which depended on the liquid viscosity. Compared with the spreading on a smooth surface with scaling index between 2/7 and 1/5,[1] the scaling indices were much larger and the spreading velocities were much faster. This is because the pillars accelerated the liquid, causing the lyophilic surface to become superlyophilic.

How did these micropillars accelerate the liquid and make the liquid superwet the solid? We used a high-magnification microscope to reveal the details in spreading (Fig. 8). Driven by the surface tension, the contact line moved along its normal at first. Once getting in touch with the pillars at 0.2 ms, the liquid began to spread along the pillars. The radius of curvature of the liquid in the inset was about 2 μm in the order of w. Hence, the local Laplace pressure $P_{c1} \sim \gamma_{LV}/w \sim 10^3$ Pa, which provided additional driving energy to pull the liquid to spread with a fast velocity along the corner between the pillars and the substrate.[32] The liquid near the pillars quickly accommodated to the square shape and was pinned by the pillars at 0.4 ms. Meanwhile, the rest part of the MCL still kept spreading in a line with a slow velocity. As a result, a local Laplace pressure $P_{c2} \sim \gamma_{LV}/p \sim 10^2$ Pa was formed and made the MCL to be a wavy line at 0.8 ms. The local radius of curvature trended to become larger at 1.6 ms. The fast and slow part of the MCL tried to reach a balance state and return a line finally. This process repeated in every period. The Laplace pressures at the interior corner and at the wavy MCL are the answers to the superwetting on the pillar-arrayed surface.

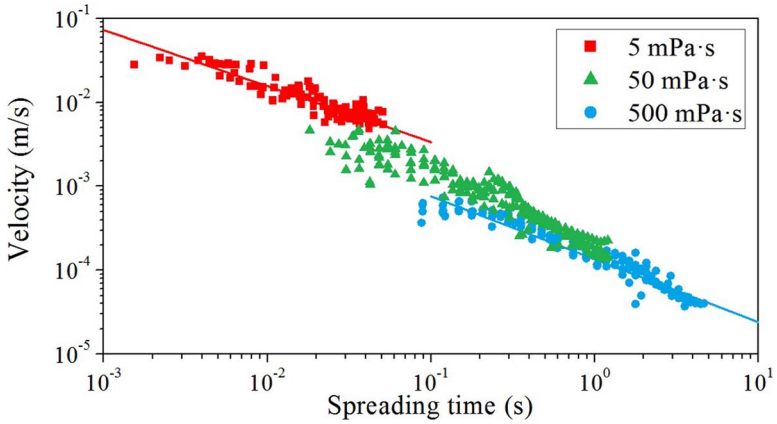

FIG. 7. The evolution of the spreading velocity with respect to time of droplets with viscosities of 5 mPa s (red squares), 50 mPa s (green triangles), and 500 mPa s (blue circles) on pillar-arrayed surfaces, respectively. The colored points represent data for samples in Table I. The red and blue lines represent the scaling laws $U \sim t^{-2/3}$ and $U \sim t^{-3/4}$, respectively.

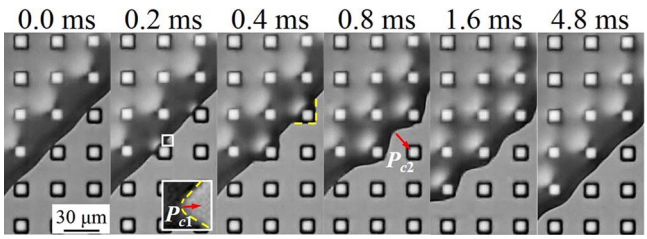

FIG. 8. Sequence snapshots of liquid ($\mu = 5$ mPa s) spreading on pillar-arrayed surfaces (sample 3 in Table I). The inset shows a close-up image of radius of curvature of the liquid labeled by a yellow dashed line. P_{c1} and P_{c2} represent the local capillary pressures.

The inertial force plays a part in the spreading dynamics. For the low-viscosity situations, according to Fig. 7, the absolute spreading velocity U of liquid with viscosity of 5 mPa s is at the order of 10^{-2} m/s. The corresponding inertial force $\rho U^2 \sim 10^{-1}$ Pa, while the interface force $\gamma_{LV}/L \sim 10^3$ Pa, the viscous force $\mu U/L \sim 10^0$ Pa, and the molecular-friction force $\zeta U/L \sim 10^6$ Pa, where the density $\rho \sim 10^3$ kg/m^3, surface tension $\gamma_{LV} \sim 10^{-2}$ N/m, viscosity $\mu \sim 10^{-3}$ Pa s, the coefficient of molecular friction $\zeta \sim 10^3$ Pa s,[33] and characteristic length $L \sim 10^{-5}$ m. In this paper, we focus on the main effects and obtain the scaling laws. The inertial effect is not the main effect, however it would also affect the dynamic process in the low-viscosity cases, which needs further consideration and systematic studies. With the increase of the viscosity of the liquid, the absolute spreading velocity decreases, and the inertial effect decreases accordingly.

B. Scaling analysis

To reveal the underlying mechanism of the viscosity-dependent scaling laws of a droplet spreading on the pillar-arrayed surface, we proposed a combined model of the hydrodynamics and the molecular kinetic theory to take account of energy dissipated by both the viscous resistance at mesoscale and the molecular friction at microscale. The spreading speed is controlled by the balance of the rate of change in the driving energy F and energy dissipation D, i.e., $F = D$. In our case, the droplet is sufficiently small, the gravitational force could be ignored compared with the surface tension. Therefore, the rate of change in interface energy per unit length of the MCL is $F = [(\gamma_{SV} - \gamma_{SL}) \cdot ro - \gamma_{LV} \cos\theta]\, U$, where γ_{SL}, γ_{SV}, and γ_{LV} are the solid-liquid, solid-vapor, and liquid-vapor interface energies, respectively. θ is the instant contact angle. Taking account of the Young's equation ($\gamma_{SV} - \gamma_{SL} = \gamma_{LV} \cos\theta_0$, where θ_0 is the static contact angle),[34] $F = \gamma_{LV} U\,(ro \cdot \cos\theta_0 - \cos\theta)$. Adopting the lubrication approximation ($H_b \ll R_b$, $\theta \sim H_b/R_b \sim 0$),[35] $F \sim \gamma_{LV} U\theta^2$.

The energy dissipation in the triple-phase region arises from two aspects: the viscous resistance D_{vis} owing to the viscous bending at mesoscale and the molecular friction D_{mol} owing to the adsorption/desorption of liquid molecules on the solid surface at microscale. First, let us discuss D_{vis}, which is a weighted average of those occurring on the top surfaces D_b, side walls of the pillars D_s, and the substrate D_f (Fig. 2). The rate of viscous dissipation per unit volume in a fluid with viscosity μ is $\varepsilon \approx \mu(\mathrm{d}u/\mathrm{d}z)^2 = \mu[U/h(r)]^2$,[36] where $h(r) \approx \theta r$ for small θ considering the lubrication approximation,[35] and r is the distance from the liquid wedge. Integrating ε_b (the rate of viscous dissipation per unit volume in the bulk) over the wedge on the top surface of the pillars, we can estimate $D_b \approx \int_{H_f}^{H_b+H_f} \varepsilon_b h_b \mathrm{d}r = \mu U^2 \int_{H_f}^{H_b+H_f} \mathrm{d}r/h_b \approx \mu U^2 \ln\left[\left(H_b + H_f\right)/H_f\right]/\theta$. In the same way, the energy dissipation on the substrate can be estimated as $D_f \approx \int_{L_m}^{H_f} \varepsilon_f h_f \mathrm{d}r = \mu U^2 \int_{L_m}^{H_f} \mathrm{d}r/h_f$. Because $p \sim H_f$, $\mathrm{d}h_f/\mathrm{d}r \gg \theta$, resulting in $D_f \ll D_b$. Hasimoto has already estimated the energy dissipation on the side walls of pillars, $D_s \approx \mu U^2/\ln(p/w)$.[21] Because $\ln(p/w) \sim 1 \gg \theta/\ln\left[\left(H_b + H_f\right)/H_f\right]$, $D_s \ll D_b$. So, the total viscous dissipation $D_{vis} \approx \mu U^2 \ln\left(H_b/H_f\right)/\theta$. The energy dissipation owing to the molecular friction is described in MKT $D_{mol} \sim U^2\zeta$, where $\zeta = k_B T/\kappa_0\lambda^3$ is the coefficient of molecular friction.

When a droplet is deposited on the pillars, the initial spherical droplet with radius R_0 evolves into the bulk and the fringe. For the sake of mass conservation, $V_0 = V_b + V_f$, i.e., $4\pi R_0^3/3 = \pi H_b \left(3R_b^2 + H_b^2\right)/6 + \pi (1-\phi_s) H_f R_f^2$, where R_b and R_f are, respectively, the average radius of the bulk and the fringe, ϕ_s is the density of roughness ($\phi_s = w^2/p^2$ for pillars). In the spreading process, $\alpha R_b \sim R_f \sim R$ is validated in the previous works,[12,37] where α ($\alpha \leq 1$) is independent of time. So $\theta \sim H_b/R_b \sim \left(4R_0^3 - 3\bar{h}R^2\right)/R^3$, where $\bar{h} = (1-\phi_s) H_f$.

Based on the above estimates of the energies and geometric relations, we arrive at the derivation of scaling laws of a droplet on pillar-arrayed surfaces.

$$U = \dot{R} \sim \frac{\gamma_{LV}\theta^3}{C\mu + \zeta\theta} \sim \frac{\gamma_{LV}\left(4R_0^3/R^3 - 3\bar{h}/R\right)^3}{C\mu + \zeta\left(4R_0^3/R^3 - 3\bar{h}/R\right)}, \tag{1}$$

where C is a constant in our cases.

In Eq. (1), the terms $(4R_0^3/R^3)$ and $(3\bar{h}/R)$ represent the contributions of the bulk droplet and the surface roughness, respectively. From Eq. (1), two extreme regimes could be distinguished: one is for the smooth surface and the other is for the rough surface.

(1) Smooth surface, i.e., relative large droplet, short or sparse pillars. The effect of surface roughness is negligible, so we neglect term $(3\bar{h}/R)$ in Eq. (1) and obtain the governing equation for a droplet on smooth surfaces

$$\dot{R} \sim \frac{\gamma_{LV}\left(4R_0^3/R^3\right)^3}{C\mu + 4\zeta R_0^3/R^3}. \tag{2}$$

When the viscous resistance is dominant, $\dot{R} \sim U_{c,v} R_0^9/R^9$, where the capillary velocity $U_{c,v} = \gamma_{LV}/\mu$. The dimensionless solution is $R/R_0 \sim \left(t/\tau_{c,v}\right)^{1/10}$, where the characteristic time $\tau_{c,v} = \mu R_0/\gamma_{LV}$ is only controlled by the properties of the droplet R_0, γ_{LV}, and μ. When the molecular friction is dominant, $\dot{R} \sim U_{c,m} R_0^6/R^6$, where $U_{c,m} = \gamma_{LV}/\zeta$ is the molecular capillary velocity. The dimensionless solution is $R/R_0 \sim \left(t/\tau_{c,m}\right)^{1/7}$, where the characteristic time $\tau_{c,m} = \zeta R_0/\gamma_{LV}$ is controlled by not only properties of the droplet R_0 and γ_{LV}, but also property of the solid-liquid interface ζ. These results are analogous to those described by previous works,[8,9] and have been examined by a variety of experiments[7] and simulations.[38]

(2) Rough surface, i.e., relative small droplet, long or dense pillars. The effect of surface roughness dominates the dynamic wetting process, so we neglect term $(4R_0^3/R^3)$ in Eq. (1) and obtain the governing equation for a droplet on pillar-arrayed surfaces

$$\dot{R} \sim \frac{\gamma_{LV}\left(3\bar{h}/R\right)^3}{C\mu - 3\zeta\bar{h}/R}, \tag{3}$$

and three scenarios are possible.

(a) When viscous resistance takes priority, $\dot{R} \sim \gamma_{LV}\bar{h}^3/\mu R^3$, the dimensionless solution is $R/R_0 \sim \left(t/\tau_{c,v}^r\right)^{1/4}$. The characteristic time $\tau_{c,v}^r = \mu R_0^4/\gamma_{LV}\bar{h}^3$ is controlled not only by properties of the droplet R_0 and $U_{c,v}$, but also by the topology of the pillars $\bar{h} = (1-\phi_s) H_f$. The consequent scaling law of spreading area is $S \sim t^{1/2}$.

(b) When molecular friction takes priority, $\dot{R} \sim \gamma_{LV}\bar{h}^2/\zeta R^2$, the dimensionless solution is $R/R_0 \sim \left(t/\tau_{c,m}^r\right)^{1/3}$. The characteristic time $\tau_{c,m}^r = \zeta R_0^3/\gamma_{LV}\bar{h}^2$ is controlled by properties of the droplet R_0 and γ_{LV}, property of the solid-liquid interface ζ, as well as the topology of the pillars ϕ_s and H_f. The consequent spreading area $S \sim t^{2/3}$ and is corroborated in our experiments shown in Fig. 6(a).

(c) Both viscous resistance and molecular friction contribute to the energy dissipation and govern the spreading process. So, the dimensionless solution is $R/R_0 \sim \left(t/\tau_c^r\right)^n$, where $1/4 < n < 1/3$ depends on their proportion in the total energy dissipation. With the increase of μ/ζ, the scaling exponent n gradually increases from 1/4 to 1/3. The consequent spreading area $S \sim t^{2n}$ is shown in Fig. 6(b).

The above theoretical results are validated in our experiments shown in Fig. 6. With lower viscosity, the liquid spreads faster with a larger scaling exponent of 2/3; with higher viscosity, the liquid spreads slower with a smaller exponent of 1/2. The velocity increases faster than the decrease of the viscosity.

IV. CONCLUSION

We have experimentally studied the spreading dynamics of a droplet on micropillar-arrayed surfaces. Because of the competition between the viscous resistance at mesoscale and the molecular friction at microscale, the spreading shape and scaling exponent change with the variation of the liquid viscosity. When the viscosity is small, the molecular friction dominates and energy mainly dissipates when liquid molecules adsorb and desorb on the solid at MCL. With the increase of the viscosity, the effect of the viscous resistance increases. When the viscosity is large, the viscous resistance dominates and energy mainly dissipates when the meniscus bends in the triple-phase region. We theoretically obtained the governing equation for dynamic spreading of a droplet, which takes account of the combined influences of the viscous resistance and the molecular friction. Scaling laws for different cases were derived and experimentally validated. The details in the dynamic spreading process were revealed. The Laplace pressures at the interior corner and at the wavy MCL were the answers to superwetting on the pillar-arrayed surface. Under the drive of the excess driving energy, the fringe separated from the droplet and penetrated into the gaps among the pillars. Our results may help to understand the dynamic spreading on microtextured surfaces and assist the future design of engineered surfaces in practical applications.

ACKNOWLEDGMENTS

This work was jointly supported by the National Natural Science Foundation of China (NSFC, Grant Nos. 11202213 and 11372313), the Key Research Program of the Chinese Academy of Sciences (Grant No. KJZD-EW-M01), and the Instrument Developing Project of the Chinese Academy of Sciences (Grant No. Y2010031).

APPENDIX: THREE-DIMENSIONAL SPREADING PROFILES

When light moves from a medium with a regractive index n_1 into another medium with n_2, reflection and refraction may happen. The relationship between the angles of incidence, reflection, and refraction is described by the law of reflection $\theta_i = \theta_r$, and Snell's law $n_1 \sin\theta_i = n_2 \sin\theta_t$. The relationship between the incident energy E_I, reflection energy E_R, and transmision energy E_T is described by the Fresnel equations

$$E_R = f_R E_I \quad \text{and} \quad E_T = f_T E_I \tag{A1}$$

where

$$f_R = \frac{1}{2}\left[\left(\frac{n_1 \cos\theta_i - n_2 \cos\theta_t}{n_1 \cos\theta_i + n_2 \cos\theta_t}\right)^2 + \left(\frac{n_1 \cos\theta_t - n_2 \cos\theta_i}{n_1 \cos\theta_t + n_2 \cos\theta_i}\right)^2\right] \text{ and } f_T = 1 - f_R \tag{A2}$$

are the reflectance and the transimittance, respectively.

When light moves from the air through a PDMS membrane along the normal of the PDMS surface, $E_{T1} = f_{T1} E_I$, where f_{T1} is a constant (Fig. 9(a)). When light moves from the air through a liquid wedge and a PDMS membrane, $E_{T2} = f_{T2}(\theta) E_I$, where $f_{T2}(\theta)$ is a function of the wedge angle θ (Fig. 9(b)) and could be derived from Eqs. (A1) and (A2). So, we can get

$$\frac{E_{T2}}{E_{T1}} = \frac{f_{T2}(\theta)}{f_{T1}}. \tag{A3}$$

Substituting Eqs. (A1) and (A2) into Eq. (A3), we can obtain $\tan(\theta) = \Psi(E_{T2}/E_{T1})$, where E_{T1} and E_{T2} are proportional to the gray scale of a point x in the experimental snapshots when liquid did

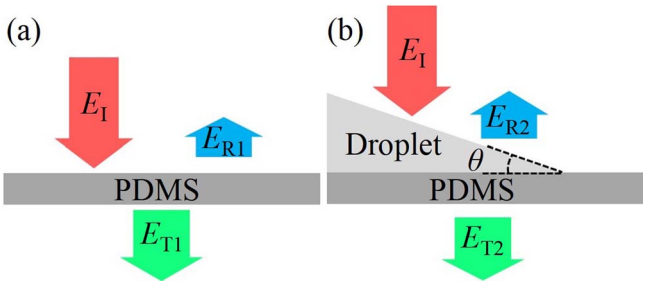

FIG. 9. Illustrations of total incident energy E_I, the reflection energy E_R, and transmission energy E_T of the light when the light moves from the air through (a) a PDMS membrane, and (b) a liquid wedge and a PDMS membrane.

not and did flow over the PDMS substrate, respectively. In this way, the spreading profile could be obtained

$$z(x) = \int_0^x z'(t)\mathrm{d}t = \int_0^x \tan(\theta)\mathrm{d}t = \int_0^x \Psi\,(E_{T2}/E_{T1})\mathrm{d}t. \tag{A4}$$

[1] D. Bonn, J. Eggers, J. Indekeu, J. Meunier, and E. Rolley, "Wetting and spreading," Rev. Mod. Phys. **81**, 739–805 (2009).
[2] P. G. De Gennes, "Wetting: Statics and dynamics," Rev. Mod. Phys. **57**, 827–863 (1985).
[3] Y. P. Zhao, "Moving contact line problem: Advances and perspectives," Theor. Appl. Mech. Lett. **4**, 034002 (2014).
[4] R. Cox, "The dynamics of the spreading of liquids on a solid surface. Part 1. Viscous flow," J. Fluid Mech. **168**, 169–194 (1986).
[5] L. Tanner, "The spreading of silicone oil drops on horizontal surfaces," J. Phys. D: Appl. Phys. **12**, 1473–1484 (1979).
[6] T. D. Blake and J. M. Haynes, "Kinetics of liquid/liquid displacement," J. Colloid Interface Sci. **30**, 421–423 (1969).
[7] P. Petrov and I. Petrov, "A combined molecular-hydrodynamic approach to wetting kinetics," Langmuir **8**, 1762–1767 (1992).
[8] F. Brochard-Wyart and P. De Gennes, "Dynamics of partial wetting," Adv. Colloid Interface Sci. **39**, 1–11 (1992).
[9] M. De Ruijter, J. De Coninck, and G. Oshanin, "Droplet spreading: Partial wetting regime revisited," Langmuir **15**, 2209–2216 (1999).
[10] D. Quéré, "Wetting and roughness," Annu. Rev. Mater. Res. **38**, 71–99 (2008).
[11] G. Mchale, N. Shirtcliffe, S. Aqil, C. Perry, and M. Newton, "Topography driven spreading," Phys. Rev. Lett. **93**, 036102 (2004).
[12] Q. Z. Yuan and Y. P. Zhao, "Multiscale dynamic wetting of a droplet on a lyophilic pillar-arrayed surface," J. Fluid Mech. **716**, 171–188 (2013).
[13] C. Ybert, C. Barentin, C. Cottin-Bizonne, P. Joseph, and L. Bocquet, "Achieving large slip with superhydrophobic surfaces: Scaling laws for generic geometries," Phys. Fluids **19**, 123601 (2007).
[14] A. Busse, N. D. Sandham, G. Mchale, and M. I. Newton, "Change in drag, apparent slip and optimum air layer thickness for laminar flow over an idealised superhydrophobic surface," J. Fluid Mech. **727**, 488–508 (2013).
[15] P. Papadopoulos, L. Mammen, X. Deng, D. Vollmer, and H.-J. Butt, "How superhydrophobicity breaks down," Proc. Natl. Acad. Sci. U.S.A. **110**, 3254–3258 (2013).
[16] E. Dressaire, L. Courbin, A. Delancy, M. Roper, and H. A. Stone, "Study of polygonal water bells: Inertia-dominated thin-film flows over microtextured surfaces," J. Fluid Mech. **721**, 46–57 (2013).
[17] A. R. Parker and C. R. Lawrence, "Water capture by a desert beetle," Nature **414**, 33–34 (2001).
[18] S. Nagrath, L. V. Sequist, S. Maheswaran, D. W. Bell, D. Irimia, L. Ulkus, M. R. Smith, E. L. Kwak, S. Digumarthy, and A. Muzikansky, "Isolation of rare circulating tumour cells in cancer patients by microchip technology," Nature **450**, 1235–1239 (2007).
[19] T.-S. Wong, S. H. Kang, S. K. Tang, E. J. Smythe, B. D. Hatton, A. Grinthal, and J. Aizenberg, "Bioinspired self-repairing slippery surfaces with pressure-stable omniphobicity," Nature **477**, 443–447 (2011).
[20] A. W. Martinez, S. T. Phillips, and G. M. Whitesides, "Three-dimensional microfluidic devices fabricated in layered paper and tape," Proc. Natl. Acad. Sci. U.S.A. **105**, 19606–19611 (2008).
[21] H. Hasimoto, "On the periodic fundamental solutions of the Stokes equations and their application to viscous flow past a cubic array of spheres," J. Fluid Mech. **5**, 317–328 (1959).
[22] C. Ishino, M. Reyssat, E. Reyssat, K. Okumura, and D. Quéré, "Wicking within forests of micropillars," Europhys. Lett. **79**, 56005 (2007).
[23] N. Srivastava, C. Din, A. Judson, N. C. Macdonald, and C. D. Meinhart, "A unified scaling model for flow through a lattice of microfabricated posts," Lab Chip **10**, 1148–1152 (2010).
[24] R. Xiao and E. N. Wang, "Microscale liquid dynamics and the effect on macroscale propagation in pillar arrays," Langmuir **27**, 10360–10364 (2011).
[25] S. J. Kim, J. Kim, M.-W. Moon, K.-R. Lee, and H.-Y. Kim, "Experimental study of drop spreading on textured superhydrophilic surfaces," Phys. Fluids **25**, 092110 (2013).

[26] C. Semprebon, P. S. H. Forsberg, C. Priest, and M. Brinkmann, "Pinning and wicking in regular pillar arrays," Soft Matter **10**, 5739–5748 (2014).
[27] See http://www.shinetsu.co.jp/ for Shin-Etsu Chemical Company, Asahi Seimei Otemachi Bldg.,6-1, Ohtemachi 2-chome, Chiyoda-ku, Tokyo 100-0004, Japan.
[28] Q. Z. Yuan and Y. P. Zhao, "Precursor film in dynamic wetting, electrowetting, and electro-elasto-capillarity," Phys. Rev. Lett. **104**, 246101 (2010).
[29] C. Wang, H. Lu, Z. Wang, P. Xiu, B. Zhou, G. Zuo, R. Wan, J. Hu, and H. P. Fang, "Stable liquid water droplet on a water monolayer formed at room temperature on ionic model substrates," Phys. Rev. Lett. **103**, 137801 (2009).
[30] L. Courbin, E. Denieul, E. Dressaire, M. Roper, A. Ajdari, and H. A. Stone, "Imbibition by polygonal spreading on microdecorated surfaces," Nat. Mater. **6**, 661–664 (2007).
[31] G. Mchale, "Surface wetting: Liquids shape up nicely," Nat. Mater. **6**, 627–628 (2007).
[32] Q. Z. Yuan and Y. P. Zhao, "Topology-dominated dynamic wetting of the precursor chain in a hydrophilic interior corner," Proc. R. Soc. A **468**, 310–322 (2012).
[33] T. D. Blake, *Wettability* (Dekker, New York, 1993).
[34] T. Young, "An essay on the cohesion of fluids," Philos. Trans. R. Soc. London **95**, 65–87 (1805).
[35] H. Greenspan, "On the motion of a small viscous droplet that wets a surface," J. Fluid Mech. **84**, 125–143 (1978).
[36] L. D. Landau and E. M. Lifshitz, *Fluid Mechanics* (Pergamon, Oxford, 1987).
[37] S. J. Kim, M. W. Moon, K. R. Lee, D. Y. Lee, Y. S. Chang, and H. Y. Kim, "Liquid spreading on superhydrophilic micropillar arrays," J. Fluid Mech. **680**, 477–487 (2011).
[38] M. J. De Ruijter, T. D. Blake, and J. De Coninck, "Dynamic wetting studied by molecular modeling simulations of droplet spreading," Langmuir **15**, 7836–7847 (1999).
[39] M. Born and E. Wolf, *Principles of Optics: Electromagnetic Theory of Propagation, Interference and Diffraction of Light* (Pergamon, Oxford, 1980).